PAPER

Magnetically separable $Zn_{1-x}Co_{0.5x}Mg_{0.5x}Fe_2O_4$ ferrites: stable and efficient sunlight-driven photocatalyst for environmental remediation

Kundan Jangam,[a] Kundan Patil,[a] Sagar Balgude, [ID]*[b] Sunil Patange[c] and Paresh More*[a]

Nanomaterials have recently gained significant interest as they are believed to offer an outstanding prospect for use in environmental remediation. Among many possible candidates, due to their useful properties including magnetic nature, wide surface area, and high absorptivity, ferrite materials hold tremendous appeal, allowing them to be used for multifaceted applications. In the present study, using a sol–gel auto combustion process, a magnetically separable $Zn_{1-x}Co_{0.5x}Mg_{0.5x}Fe_2O_4$ (x = 0.0, 0.25, 0.50, 0.75, 1.0) ferrite with superior photocatalytic activity for dye degradation was manufactured. Rietveld refinement and FTIR studies confirm that a single-phase cubic spinel system was built for all samples with crystallite sizes of 34–57 nm. VSM has determined the magnetic properties of the samples at room temperature. With the introduction of Mg^{2+} and Co^{2+} in the Zn ferrites, a transformation from the soft superparamagnetic activity to the hard ferromagnetic character was reported. Considering the band structure in the visible region, the photocatalytic activities of the $Zn_{1-x}Co_{0.5x}Mg_{0.5x}Fe_2O_4$ ferrites for the degradation of the MB dye under natural sunlight were investigated. $Zn_{0.25}Co_{0.375}Mg_{0.375}Fe_2O_4$ showed an efficiency of degradation of 99.23% for MB dye with a quick 40 min irradiation period with high reusability of up to four cycles.

1. Introduction

Spinel ferrites have been extensively studied for several decades because of their versatile and promising magnetic, optical, electrical, and chemical properties, which often vary from their bulk counterpart.[1,2] Some important applications (including magnetic sensors, catalysis, MRI imaging, supercapacitors, and antibacterial agents) attract spinel ferrites.[3–7] Recently, research studies have more focused on the synthesis of spinel ferrites with a general formula of AFe_2O_4, where A stands for metals, such as Co, Mg, Zn, Ni, Mn. Several forms of magnetic ferrites, such as manganese ferrite ($MnFe_2O_4$), cobalt ferrite ($CoFe_2O_4$), zinc ferrite ($ZnFe_2O_4$), and copper ferrite ($CuFe_2O_4$), have been reported to exhibit excellent catalytic and photocatalytic operation. Various chemical methods have been thoroughly investigated for the synthesis of well-dispersed spinel ferries, such as solvothermal, chemical co-precipitation, microwave, and sol–gel auto combustion.[8–11] Due to its simplicity, lower time and energy, and environmental safety, the sol–gel auto combustion

method has attracted considerable attention among the various methods.

In the past decade, environmental pollution has increased the extreme overall anxiety. For instance, the release of industrial wastewater containing synthetic pigments, phenolic derivatives, and organic colouring contributes to significant environmental hazards. These contaminants are non-degradable and thus cause the aquatic life to have a serious problem. Nanomaterials play a very vital role in the degradation of effluents released from dyes and textile industries.[12,13] As photocatalysts that act as sensitizers for light-induced redox processes, various semiconducting materials (such as TiO_2, ZnO, and Sn_3O_4) have customarily been used.[14–16] Recently, spinel ferrites are important photocatalysts used for environmental remediation.[17,18] Its stability, abundant availability, non-toxicity, and simple synthesis make it an economically and environmentally interesting choice for the removal of aqueous organic contaminants in AOPs.[19–21] The spinel ferrites exhibit a bandgap in the visible region. In view of the bandgap in the visible region, several researchers have synthesized various ferrites, and researched their morphological and optical properties. For example, Cao *et al.* studied the photocatalytic degradation of the MB dye using the CES-derived zinc ferrite,[22] and Yang *et al.* demonstrated the fabrication of Cr and Mn-doped zinc ferrite nanospheres using industrial waste. The synthesized ferrites were tested for the degradation of Congo

[a]*Department of Chemistry, K. E. T's, V. G. Vaze College, Maharashtra, India. E-mail: paresh.m34@gmail.com*

[b]*Department of Chemistry, D. Y. Patil University, Maharashtra, India. E-mail: sagarbalgude88@gmail.com*

[c]*Department of Physics, Shrikrishna Mahavidyalaya Gunjoti, Maharashtra, India*

red dye.[23] Mohammad *et al.* reported the hydrothermal route for the synthesis of cobalt ferrites, revealing an enhanced activity for the degradation of Reactive red 4 dye.[24] Borhan *et al.* designed the $ZnFe_{2-x}Al_xO_4$ ferrites using the sol–gel auto combustion method for the photodegradation of Orange I dye.[25] Mahmoodi *et al.* reported the degradation of Reactive red 120 and Reactive red 198 dye using magnetically separable zinc ferrites.[26] Satya *et al.* studied the removal of cationic triaryl-methane dyes in contaminated water using spinel cobalt ferrites.[27] Ikram *et al.* have reported on $CoFe_2O_4$ and $MnFe_2O_4$ nanocrystals by microwave-assisted and co-precipitation methods, respectively, and the catalyst showed excellent results in the photodegradation of the MB dye.[28] These studies highlighted that while some great work has been done on photocatalysis, the catalytic performance remains unsatisfactory, and further work is still needed to explore new approaches to improve it. In this context, the present work is the first report on the synthesis of $Zn_{1-x}Co_{0.5x}Mg_{0.5x}Fe_2O_4$ ferrites and its photocatalytic activity under natural sunlight.

Herein, we synthesized $Zn_{1-x}Co_{0.5x}Mg_{0.5x}Fe_2O_4$ ferrites using a cost-effective and simple sol–gel auto combustion method. The photocatalytic activity of the as-synthesized ferrites under solar light irradiation was tested for degradation of the methylene blue dye. The magnetic, physicochemical, optical, and morphological properties of the as-synthesized $Zn_{1-x}Co_{0.5x}Mg_{0.5x}Fe_2O_4$ ferrites were elucidated by characterization using various analytical techniques. A plausible photocatalytic mechanism for the degradation of the MB dye in the $Zn_{1-x}Co_{0.5x}Mg_{0.5x}Fe_2O_4$ ferrites was also suggested.

2. Experimental details

2.1 Synthesis

$Zn(NO_3)_2 \cdot 6H_2O$, $Co(NO_3)_2 \cdot 6H_2O$, $Mg(NO_3)_2 \cdot 6H_2O$, and $Fe(NO_3)_3 \cdot 9H_2O$ were procured from Merck (India). Cobalt and magnesium-doped $Zn_{1-x}Co_{0.5x}Mg_{0.5x}Fe_2O_4$ ($x = 0.0, 0.25, 0.50, 0.75, 1.0$) ferrites were synthesized using the sol–gel auto combustion method. During synthesis, the aqueous solution was prepared by taking all of the nitrates and glycine in a 1 : 3 molar ratio in water. The as-formed homogeneous mixture was stirred well, and the pH of the reaction mixture was adjusted to 7–8 with liq. NH_3 to form "sol". To obtain a viscous gel, the viscous fluid was condensed or hardened to form the 'gel', and the sol was placed on the hot plate at 90 °C. On the hot plate, this homogeneous gel was ignited. The glycine was then completely combusted, yielding $Zn_{1-x}Co_{0.5x}Mg_{0.5x}Fe_2O_4$ ferrites. The as-synthesized samples of ferrites were ground well, and then annealed in the furnace at 800 °C for five hours. The obtained samples were labeled as ZF1 ($X = 0.0$), ZCMF1 ($X = 0.25$), ZCMF2 ($X = 0.50$), ZCMF3 ($X = 0.75$) and as CMF ($X = 1.0$), respectively, and were characterized using various techniques.

2.2 Characterization

This XRD pattern of the $Zn_{1-x}Co_{0.5x}Mg_{0.5x}Fe_2O_4$ ferrites was recorded on Philips (Xpert) X-ray diffractometer using Cu K_α radiation having wavelength 1.540 Å at room temperature. The morphology investigation of the $Zn_{1-x}Co_{0.5x}Mg_{0.5x}Fe_2O_4$ ferrites can be done using JEOL JSM-7600F, FEG-SEM instrumentation. The optical properties were recorded by UV-visible spectrophotometer (Shimadzu make model 1800). The analysis of the magnetic properties was carried out by Quantum Design USA to make the SQUID system (Model MPMS XL). FTIR spectra of all samples were recorded on a 3000 Hyperion Microscope with vertex 80 FTIR using KBr pellets in the range of 400 to 4000 cm^{-1}.

2.3 Photocatalytic activity

The as-synthesized $Zn_{1-x}Co_{0.5x}Mg_{0.5x}Fe_2O_4$ ferrites were tested using methylene blue (MB) dye as a model contaminant for its photodegradation behavior. For the photoreactor, the Pyrex beaker used was 250 mL. To ensure healthy adsorption, 100 mL, 10 ppm aqueous MB dye solution containing 0.2 g of the catalyst was stirred in the dark before sunlight irradiation. They were exposed to sunlight after 1 hour of suspension. Reaction samples were collected at regular intervals, and a UV-visible spectrophotometer was used to check the residual MB dye content.

3. Results & discussion

The crystalline structure of the $Zn_{1-x}Co_{0.5x}Mg_{0.5x}Fe_2O_4$ ferrites was investigated by the Rietveld refinement XRD pattern. Fig. 1 shows the XRD and Rietveld refinement patterns of cobalt and magnesium-doped $Zn_{1-x}Co_{0.5x}Mg_{0.5x}Fe_2O_4$ ($x = 0.0$ to 1.0) ferrites. Form the figure, all diffraction peaks in the XRD spectra were indexed to the (111), (220), (311), (222), (400), (422), (511), and (440) planes of the cubic spinel phase. The measured diffraction peaks of ZF, ZCMF1, ZCMF2, ZCMF3, and CMF ferrites are in accordance with JCPDS card no. 22-1012.[29] The as-synthesized ferrites are polycrystalline in a single phase without any other impurity phases. It can also be found that the substitution of Zn by the substance of Co–Mg does not alter the structure of the cubic spinel zinc ferrite.

The efficiency of refinement is defined by the consideration of the goodness-of-fit (χ^2). The findings obtained in the Rietveld refinement on the X-ray diffraction of the $Zn_{1-x}Co_{0.5x}Mg_{0.5x}Fe_2O_4$ ferrites systems are listed in Table 1. From Table 1, the Rietveld refinement of the goodness-of-fit (χ^2) ranged from 1.05 to 1.82, and the low value of the fitting factor is attributed as an excellent result value. The profile fitting is better with lower χ^2 values; hence, the procedure adopted for the profile fitting is by minimizing the χ^2 function. Fig. 2 and Table 1 demonstrate the theoretical and observed lattice constant of $Zn_{1-x}Co_{0.5x}Mg_{0.5x}Fe_2O_4$ ($x = 0.0$ to 1.0) ferrites, and the values are very much in agreement. Fig. 2 shows that the lattice parameter decreases from ($x = 0.0$ to 1.0), and that the decrease in the lattice parameters is in accordance with Vegards law.[30] Furthermore, the close observations from the figure indicate that the a_{th} value is greater than the a_{obs} value. This is because the ideal spinel structure was considered a rigid sphere for measuring the a_{th} value with cations and anions. The crystallite size of the as-
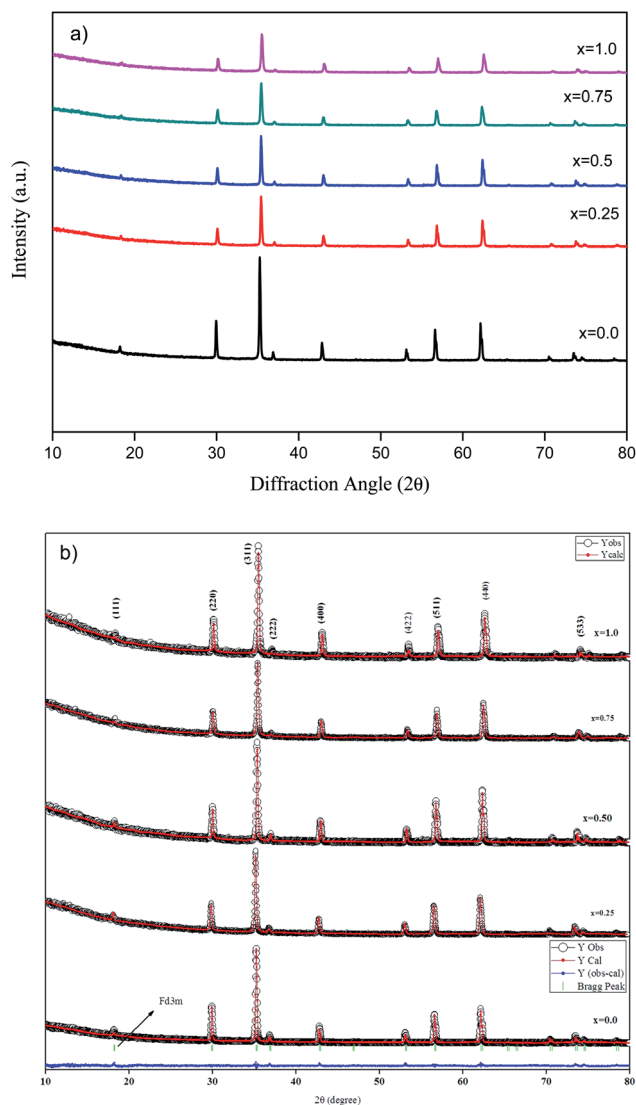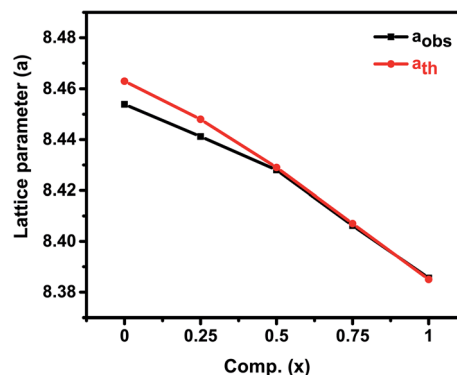
Fig. 2 Theoretical and observed lattice parameters of $Zn_{1-x}Co_{0.5x}$-$Mg_{0.5x}Fe_2O_4$ ($x = 0.0$ to 1.0) ferrites.

Fig. 1 (a) XRD and (b) Rietveld refinement spectra of $Zn_{1-x}Co_{0.5x}$-$Mg_{0.5x}Fe_2O_4$ ($x = 0.0$ to 1.0) ferrites.

synthesized ferrites was calculated using the Debye–Scherrer equation, and the most intense 311 peak was chosen for measuring the crystallite size:[30]

$$d = 0.9\lambda/\beta \cos\theta$$

where d is the size of the crystallite (nm), θ is the peak angle, λ is the wavelength of the X-ray beam, and β is the full width at half

maximum (FWHM) of prominent intense peak measured in radians. The size of the crystallite decreases ($x = 0.0$ to 1.0), as shown in Table 1, from 57.25 nm to 34.19 nm. The decrease in the crystallite size is due to the substitution of a large ionic radius of Zn^{2+} ions with a smaller ionic radius of Co^{2+} and Mg^{2+}.[31] Sharma *et al.* reported similar variation behavior in the size of the crystallite, with very limited ion doping.[32] From the lattice parameter, the X-ray density of the $Zn_{1-x}Co_{0.5x}Mg_{0.5x}$-$Fe_2O_4$ ferrites was measured. With the increasing concentration of Co^{2+} and Mg^{2+} ($x = 0.0$ to 1.0), there is a steady decrease in the X-ray density. The decrease in the crystallinity with a decrease in the lattice parameter may be the key cause for decreasing the X-ray density.[33]

The Bertaut method was used in spinel ferrite to assess the site occupancy.[34] This is calculated from the study of the $Zn_{1-x}Co_{0.5x}Mg_{0.5x}Fe_2O_4$ ($x = 0.0$ to 1.0) X-ray diffraction pattern. The exact information on the cation distribution was obtained by comparing the intensity ratio (experimental and calculated) for the reflections, whose intensities: (i) vary with cation distribution in opposite ways, (ii) are almost independent of the oxygen position parameter, and (iii) are not significantly different. The distribution of cations at the tetrahedral site and octahedral site is shown in Table 1. The trivalent Fe^{3+} ions are distributed both at the tetrahedral and octahedral sites due to the simultaneous doping of cobalt and magnesium ions. Cobalt ions push Fe^{3+} ions to the tetrahedral sites, and this results in the distribution of Fe^{3+} ions over the tetrahedral A and octahedral B sites. However, it does show maximum occupancy at the B site. This is due to the greater ionic radius of the Zn^{2+} ion (0.82 Å). It appears to live on the tetrahedral site, and displaces

Table 1 Goodness of fit (χ^2), lattice parameter (observed (a_{obs}) and theoretical (a_{th})), radii of the tetrahedral (r_A) and octahedral (r_B) sites, oxygen position parameter (u), crystallite size (d), and X-ray density

Comp.	χ^2	a_{obs} (Å)	a_{th} (Å)	r_A (Å)	r_B (Å)	u (Å)	d (nm)	d_x (g cm^{-3})
ZF	1.82	8.4539	8.463	0.74	0.67	0.3906	57.25	5.2739
ZCMF1	1.4	8.4412	8.448	0.739	0.6702	0.3908	52.43	5.1736
ZCMF2	1.26	8.4280	8.429	0.737	0.6704	0.391	48.57	5.0878
ZCMF3	1.05	8.4062	8.407	0.736	0.6705	0.3912	42.13	4.9872
CMF	1.47	8.3856	8.385	0.735	0.6707	0.3915	34.19	4.8974

Table 2 Cation distribution of $Zn_{1-x}Co_{0.5x}Mg_{0.5x}Fe_2O_4$

		Occupancy of cations	
Comp.	Chemical formulae	A site	B site
ZF	$ZnFe_2O_4$	Zn_1	Fe_2
ZCMF1	$Zn_{0.75}Co_{0.125}Mg_{0.125}Fe_2O_4$	$Zn_{0.75}Mg_{0.0125}Co_{0.1125}Fe_{0.225}$	$Mg_{0.1125}Co_{0.0125}Fe_{1.775}$
ZCMF2	$Zn_{0.50}Co_{0.25}Mg_{0.25}Fe_2O_4$	$Zn_{0.50}Mg_{0.12}Co_{0.015}Fe_{0.365}$	$Mg_{0.13}Co_{0.235}Fe_{1.635}$
ZCMF3	$Zn_{0.25}Co_{0.375}Mg_{0.375}Fe_2O_4$	$Zn_{0.25}Mg_{0.2}Co_{0.02}Fe_{0.53}$	$Mg_{0.175}Co_{0.355}Fe_{1.47}$
CMF	$Co_{0.50}Mg_{0.50}Fe_2O_4$	$Mg_{0.3}Co_{0.025}Fe_{0.675}$	$Mg_{0.2}Co_{0.350}Fe_{1.325}$

the smaller Fe^{3+} (0.67 Å) ions and Co^{2+} (0.74 Å) ions at the expense of the Mg^{2+} (0.66 Å) ions from the tetrahedral sites to the octahedral sites. The data given in Table 2 shows that the octahedral sites are primarily occupied by Fe^{3+} ions. This is simply due to the increased energy from the octahedral sites. The radius of the tetrahedral A site (r_A) and the radius of the octahedral B site (r_B) were calculated, and are depicted in Table 1 using a modified relation discussed elsewhere.[35] With the increased concentration of cobalt and magnesium, and the decreased concentration of zinc, the r_A and r_B values increased. Similar results have been reported in the cobalt substituted in Ni–Zn ferrites.[36] The oxygen positional parameter (u) values are tabulated in Table 1. The value of the oxygen positional parameter is nearly equal to 0.375 Å in the spinel structure. The as-synthesized samples show a small increment in the oxygen positional parameter (u) value in comparison to the ideal value. These may be attributed to different causes, experimental mistakes or failures in the calculation. For most samples, $u > 0.375$ is obtained from the expansion of the tetrahedral interstitials due to the slight displacement of anions. The spatial coordinates of oxygen (u) in this series are always greater than 0.375, which can be due to the displacement of anions from the ideal positions.[35] The disturbance in the lattice is confirmed from the data of the lattice constants and oxygen positional parameters (u).

Infrared spectroscopy is an effective spectroscopic technique for obtaining information about the position of the metal ions in the crystal lattice through the presence of various vibrational modes in the crystal lattice.[37] Fig. 3a shows the FTIR spectra of the $Zn_{1-x}Co_{0.5x}Mg_{0.5x}Fe_2O_4$ ferrites. Two characteristic bands are present; the lower frequency band at 424 cm^{-1} corresponds to the intrinsic vibrations of the octahedral sites, whereas the higher frequency band at 545 cm^{-1} corresponds to the intrinsic vibrations of the tetrahedral sites. From Fig. 3b, it can be observed that with an increase in the content of Co^{2+} and Mg^{2+} (ZF to CMF), the low-frequency band (M_{tet}–O) slightly shifted to the lower frequency side, whereas the higher frequency band (M_{oct}–O) slightly shifted to the higher frequency side. These shifts are observed due to the changes in mass at sites A and B, such as replacing the tetrahedral Zn^{2+} ion with the lighter Co^{2+} and Mg^{2+} ions, at the same time as both ions transfer a few Fe^{3+} ions from the octahedral site to the tetrahedral site. The shift in the peaks of the A sites is greater than B sites, which indicates that the Co^{2+} and Mg^{2+} ions preferably go to the B sites, and some of the Fe^{3+} ions transfer to the A sites, resulting in substantial increases in the stretching tetrahedral vibrations. The same results are also confirmed from the cation distribution analysis.[38]

Morphological analysis of the as-synthesized $Zn_{1-x}Co_{0.5x}$-$Mg_{0.5x}Fe_2O_4$ ferrites was achieved using field emission scanning electron microscopy (FESEM). Fig. 4 displays the FESEM images of the as-synthesized cobalt and magnesium-doped Zn_{1-x}-$Co_{0.5x}Mg_{0.5x}Fe_2O_4$ ferrites, respectively. From Fig. 4a, it can be seen that the high magnification image at 200 nm depicts the agglomerated morphology made up of secondary irregular shaped spherical nanoparticles. The size of these nanoparticles
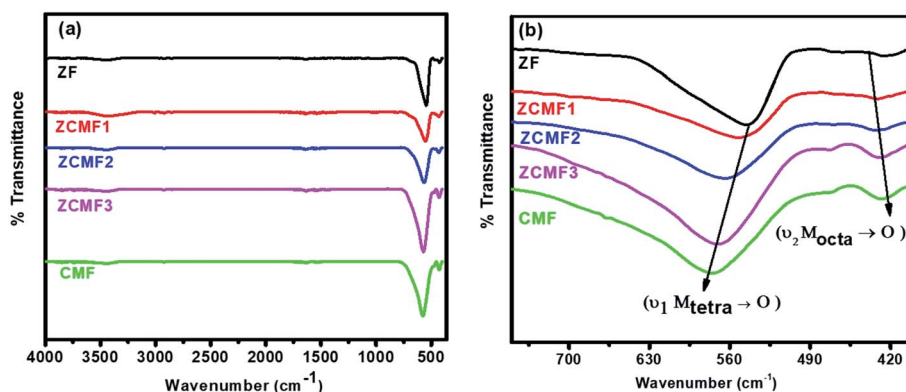

Fig. 3 FTIR absorption spectra of $Zn_{1-x}Co_{0.5x}Mg_{0.5x}Fe_2O_4$ ($x = 0.0$ to 1.0) ferrites (a) in the range of 400–4000 cm^{-1} and (b) in the range of 400 to 700 cm^{-1}.
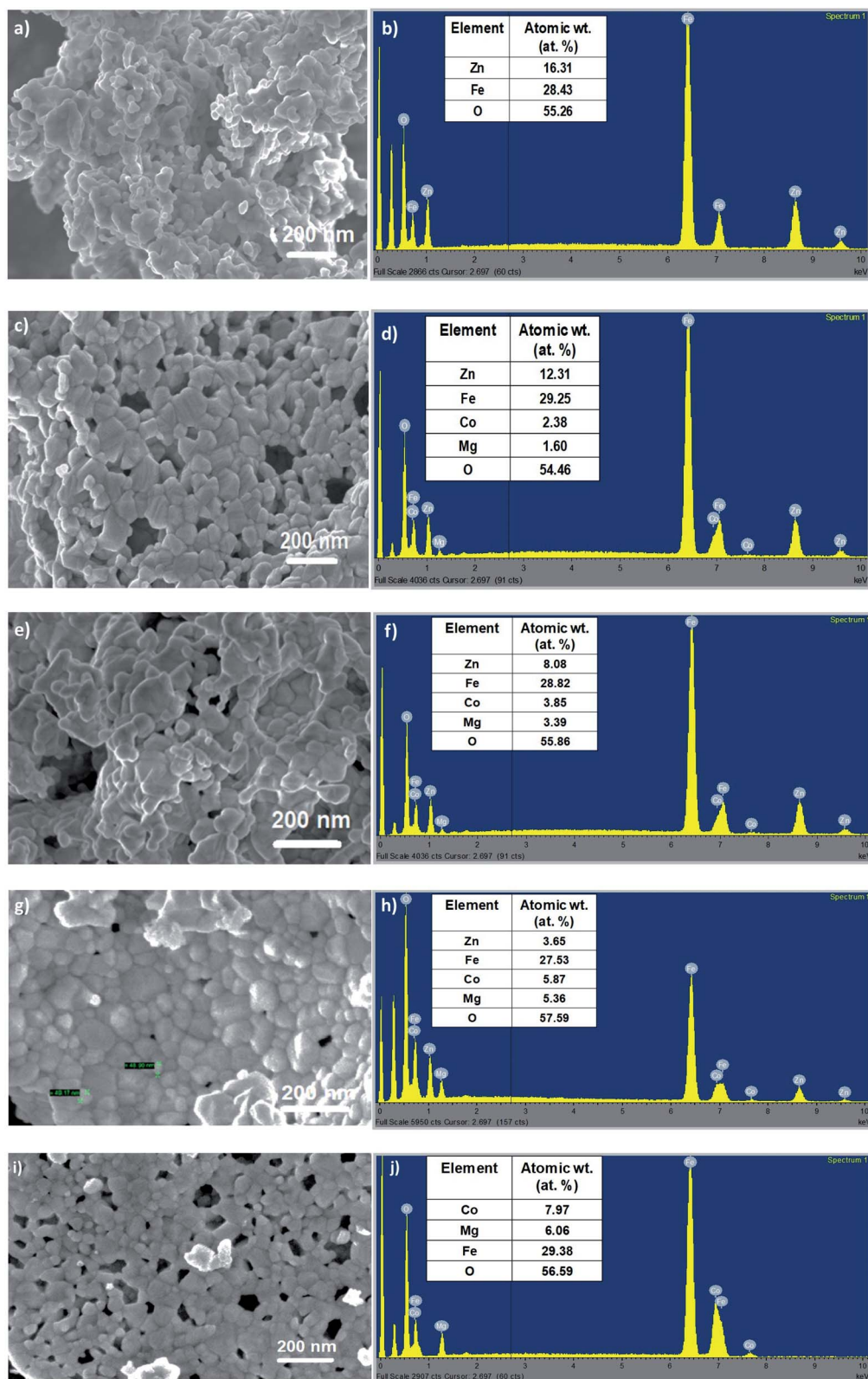
Fig. 4 FESEM and EDS images of the as-synthesized (a and b) ZF, (c and d) ZCMF1, (e and f) ZCMF2, (g and h) ZCMF3, and (i and j) CMF, respectively.

is found in the range of 40–70 nm. With cobalt and magnesium-doping in $Zn_{1-x}Co_{0.5x}Mg_{0.5x}Fe_2O_4$ (ZCMF1, ZCMF2, ZCMF3, CMF), the greater agglomeration of the spherically formed nanoparticles was observed with a subsequent reduction in the crystalline size. The agglomeration for the higher concentrations of cobalt and magnesium is due to the ferromagnetic Co^{2+}
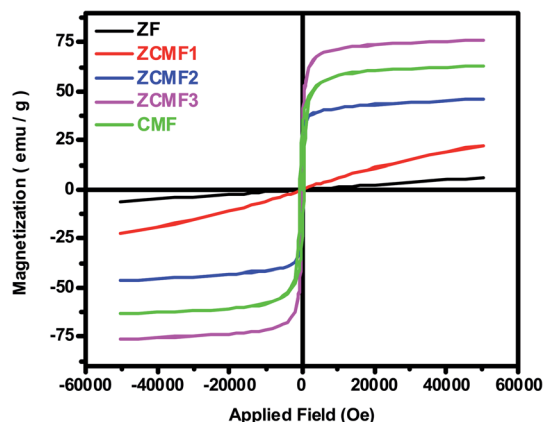
Fig. 5 Magnetic hysteresis loops of the $Zn_{1-x}Co_{0.5x}Mg_{0.5x}Fe_2O_4$ ferrites.

Table 3 Saturation magnetization (M_s), remnant magnetization (M_r), coercivity (H_c), squareness ratio (M_r/M_s), and magnetic moment (n_B) of the synthesized $Zn_{1-x}Co_{0.5x}Mg_{0.5x}Fe_2O_4$ nanoferrites at room temperature

Comp.	M_s emu g^{-1}	M_r emu g^{-1}	M_r/M_s	H_c Oe	n_B μB
ZF	6.16	0.0019	0.00031	8.32	0.26
ZCMF1	22.59	0.0097	0.00043	12.05	0.94
ZCMF2	46.27	4.1493	0.08968	26.29	1.88
ZCMF3	76.13	21.8424	0.28691	92.34	3.02
CMF	63.09	28.1948	0.4469	216.47	2.43

substitution and diamagnetic Zn^{2+} replacement. More crystallinity was observed for the undoped ZF1 sample. The agglomeration can be attributed to the magnetic nature of the samples, and this result was also confirmed by VSM analysis. Energy-dispersive X-ray analysis of the as-synthesized $Zn_{1-x}Co_{0.5x}Mg_{0.5x}Fe_2O_4$ ferrite was performed to investigate the elemental composition. Fig. 4b depicts the peaks of the Zn, Fe, O elements for undoped $ZnFe_2O_4$ (ZF1). Fig. 4d, f and h showed the peaks of the Zn, Co, Mg, Fe, O elements for ZCMF1, ZCMF2, and ZCMF3 ferrites, respectively. The sample CMF shows the peaks of Co, Mg, Fe, O elements. The stoichiometric ratios used for the synthesis of nanoferrites closely matches with the corresponding EDS results. No impurity peaks observed in the as-synthesized nanoferrites indicates the purity of the synthesized nanoferrites.

Fig. 5 shows the magnetic hysteresis loops that were recorded at room temperature for the as-synthesized $Zn_{1-x}Co_{0.5x}Mg_{0.5x}Fe_2O_4$ ferrites. The magnetic parameters obtained from the hysteresis loops, such as the remanent magnetization (M_r), saturation magnetization (M_s), coercivity (H_c), squareness ratio (M_r/M_s), and magnetic moment (n_B), are summarized in Table 3. When the Co^{2+} and Mg^{2+} dopants are introduced into a soft paramagnetic $ZnFe_2O_4$, they are transformed into hard ferrimagnetic materials. The M_s value of the $Zn_{1-x}Co_{0.5x}Mg_{0.5x}Fe_2O_4$ ferrite nanoparticles depends on the distribution of the magnetic Co^{2+} (d^7) and Fe^{3+} (d^5) ions, as well as both Mg^{2+} (d^0)

and Zn^{2+} (d^{10}) ions, which are non-magnetic in nature between the A sites (tetrahedral) and B sites (octahedral). According to the previous literature, $ZnFe_2O_4$ displays a regular spinel structure, where the Zn^{2+} ions occupy the tetrahedral (A) sites, and the octahedral (B) sites are occupied by Fe^{3+} ions. When the Zn^{2+} ions are replaced by Co^{2+} or Mg^{2+} ions, they always prefer the octahedral positions. This leads to a reverse spinal structure, and move the Fe^{3+} ions from the octahedral B sites to tetrahedral A sites.[39] This will contribute to Fe^{3+} ion redistribution on the tetrahedral and octahedral sites. In the present work, it was found that the M_s value (Fig. 6a) of the nanoparticles slowly increased with the increase of the content of Co^{2+} and Mg^{2+} until $x = 0.75$, which is observed due to the magnetic Co^{2+} ions occupying the octahedral B sites preferentially, and then unexpectedly decreased if x was greater than 0.75, i.e., CMF as indicated in Table 3. The decrease in the magnetization was observed as the concentration of the Mg^{2+} ions increased, and the non-magnetic Mg^{2+} tends to occupy the octahedral B sites that move the magnetic Fe^{3+} ions to the tetrahedral A site. The remnant magnetization (Fig. 6b) and coercivity (Fig. 6c) are gradually increased with the introduction of Co^{2+} and Mg^{2+} dopants in $ZnFe_2O_4$, which suggests that the soft magnetic materials are transformed into hard magnetic materials. Furthermore, Table 3 demonstrates the super-paramagnetic nature of samples ZF to ZCMF2 ($x = 0.0$ to $x = 0.50$), and the composition $x = 0.75$ and 1.0 (ZCMF3 and CMF) have M_r/M_s ratios greater than 0.10. Hence, these samples exhibit ferromagnetism.[40]

The UV-visible spectra of the as-synthesized $Zn_{1-x}Co_{0.5x}Mg_{0.5x}Fe_2O_4$ ferrites are shown in Fig. 7. The Tauc plot (inset: Fig. 7) of $(\alpha h\nu)^2$ against the photon energy ($h\nu$) was plotted to clarify the bandgap. The spectra show the broad absorption in the UV-visible region for the $Zn_{1-x}Co_{0.5x}Mg_{0.5x}Fe_2O_4$ ferrites, and commonly observed cubic spinel phase. The approximate ZF1, ZCMF1, ZCMF2, ZCMF3, and CMF band gaps were found to be 2.43, 2.31, 2.18, 2.01, and 2.07 eV, respectively. In addition, as the cobalt and magnesium content increased (ZCMF1 to ZCMF3), the ferrite band gap continued to decrease, supporting the substitution of the Co^{2+} and Mg^{2+} ions for Zn^{2+}. Nevertheless, a further rise in the band gap was observed at the CMF ferrite. This may be due to the complete replacement of Zn^{2+} by Co^{2+} and Mg^{2+}. All of the samples of the $Zn_{1-x}Co_{0.5x}Mg_{0.5x}Fe_2O_4$ ferrites could absorb a significant amount of sunlight due to an electronic transition from Fe 3d–O 2p.[41]

The photocatalytic efficiency of the $Zn_{1-x}Co_{0.5x}Mg_{0.5x}Fe_2O_4$ ($x = 0.00, 0.25, 0.50, 0.75, 1.0$) ferrites was studied for the degradation of methylene blue dye under natural sunlight. Fig. 8a shows the degradation of the MB dye with respect to time over the Co and Mg doped $Zn_{1-x}Co_{0.5x}Mg_{0.5x}Fe_2O_4$ ferrites. Furthermore, a controlled experiment without any catalyst was conducted for comparison. The MB dye was scarcely degraded in the absence of a catalyst, but MB dye degradation was observed in the presence of a photocatalyst. We note that the degradation rate of ZF is 93% within 80 min. By comparison, when the ZF ferrites are changed with the doping of cobalt and magnesium, the degradation levels of MB over the doped $Zn_{1-x}Co_{0.5x}Mg_{0.5x}Fe_2O_4$ ferrites also surprisingly increase. The
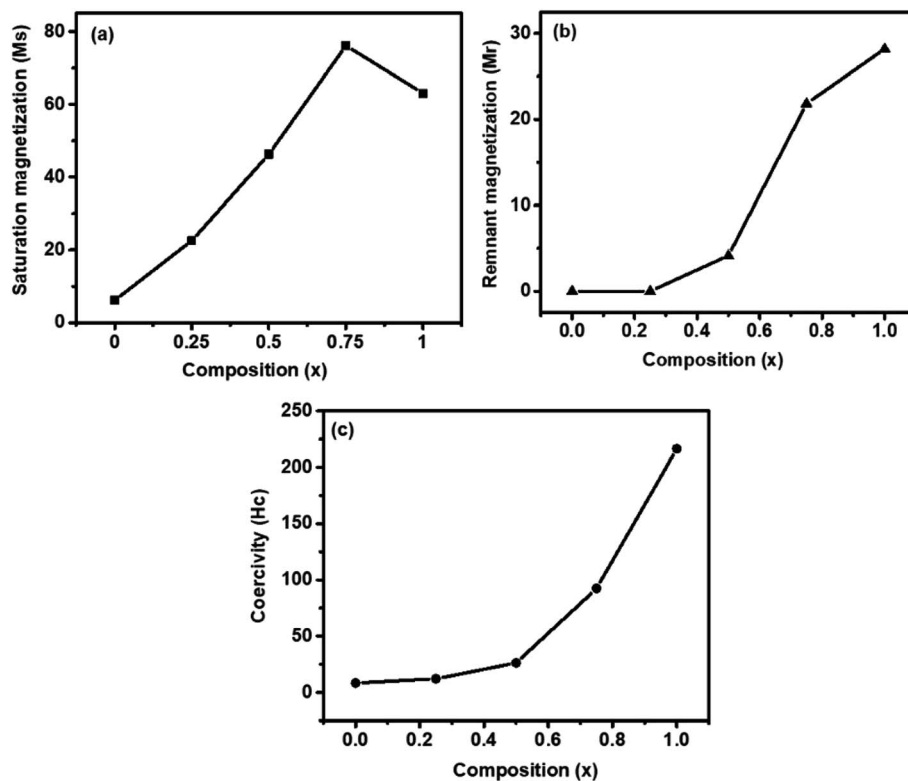
Fig. 6 VSM results of $Zn_{1-x}Co_{0.5x}Mg_{0.5x}Fe_2O_4$ ($x = 0.0$ to 1.0) ferrites: (a) saturation magnetization (M_s), (b) remanent magnetization (M_r), and (c) coercivity (H_c).
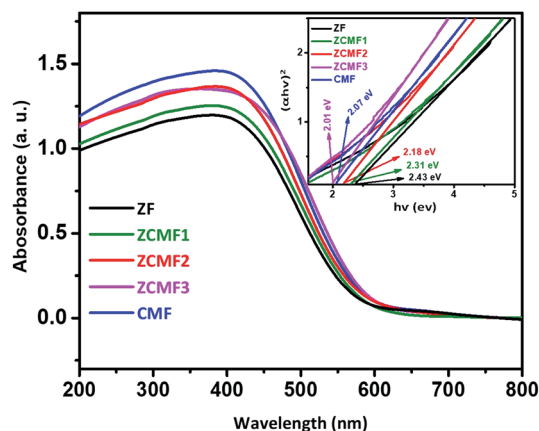

Fig. 7 UV-visible absorption spectra of $Zn_{1-x}Co_{0.5x}Mg_{0.5x}Fe_2O_4$ ($x = 0.0$ to 1.0) ferrites (inset: $(\alpha h\nu)^2$ vs. photon energy ($h\nu$) spectra for the calculation of the optical band gap by extrapolating on the $h\nu$ axis at $\alpha = 0$).

ZCMF3 sample shows the greatest amount of degradation under sunlight irradiation. The degradation rate of MB reaches up to a maximal 75% within 20 min, and completely disappeared after irradiation for 40 min. Moreover, the degradation rate was substantially higher than previous records.[42–44] However, upon further increasing the content of Co and Mg, the degradation rate starts to reduce, which could be caused by the cation distribution, as well as increase in the bandgap of CMF.

The kinetic equation of the first-order reaction is used to match the photocatalytic degradation reaction of the MB dye, in order to allow a direct quantitative comparison. The ZF, ZCMF1, ZCMF2, ZCMF3 and CMF reaction rate constants were 0.032, 0.039, 0.054, 0.108 and 0.072 min^{-1}, respectively. The ferrite rate constant of ZCMF3 is greater than that of other ferrites. Thus, the ZCMF3 ferrite has shown strong photodegradation speed with excellent linear correlation (Table 4), indicating pseudo-first-order kinetics. The improved photodegradation activity of the as-synthesized ZCMF3 ferrites may be attributed to proper band structure, morphology, and crystallinity.

The strong spectral response of the $Zn_{0.25}Co_{0.375}Mg_{0.375}Fe_2O_4$ photocatalyst was investigated for the degradation of MB dye. Fig. 8b displays the effect of catalyst loading on the MB dye degradation. The $Zn_{0.25}Co_{0.375}Mg_{0.375}Fe_2O_4$ percentage of catalyst loading by weight ranged from 0.1 g to 0.25 g. When the catalyst load is 0.15 g, the degradation of the MB dye reaches maximum (completely disappear within 45 min). Nevertheless, when increasing the content of $Zn_{0.25}Co_{0.375}Mg_{0.375}Fe_2O_4$, the rate of degradation starts to decrease, which may be attributable to the shielding effect that weakens the light harvesting ability of the photocatalyst.[45] In addition, given the stability and recyclability of the photocatalysts, we test the stability and reproducibility of $Zn_{0.25}Co_{0.375}Mg_{0.375}Fe_2O_4$ by the cyclic degradation of the MB dye under sunlight irradiation. Fig. 8c indicates that the degradation rates of the MB dye have evidently not decreased as a result of a four-fold consecutive photocatalytic reaction, indicating that $Zn_{0.25}Co_{0.375}Mg_{0.375}Fe_2O_4$ is superior
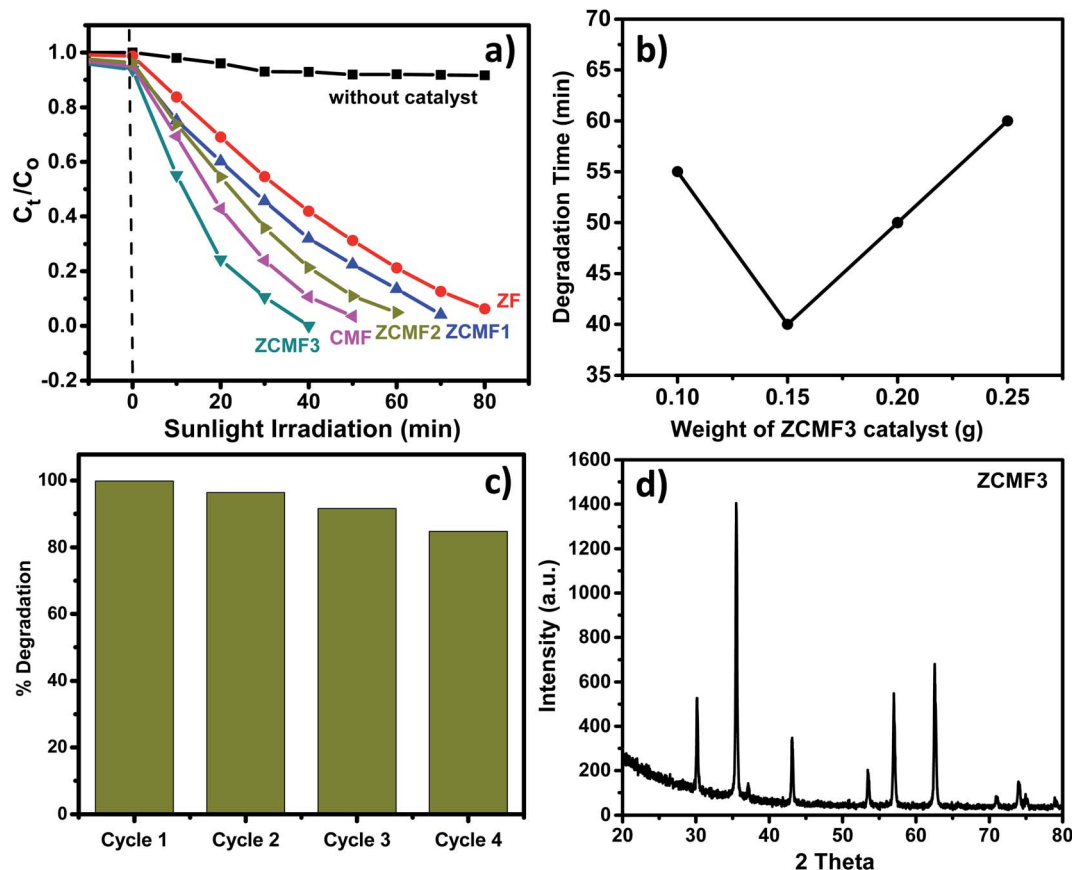
Fig. 8 (a) A plot of the change in absorbance *vs.* irradiation time in the presence of the different $Zn_{1-x}Co_{0.5x}Mg_{0.5x}Fe_2O_4$ photocatalysts. (b) Effect of catalyst loading on the $Zn_{0.25}Co_{0.375}Mg_{0.375}Fe_2O_4$ photocatalyst. (c) Recyclability of the $Zn_{0.25}Co_{0.375}Mg_{0.375}Fe_2O_4$ photocatalyst. (d) XRD spectra of $Zn_{0.25}Co_{0.375}Mg_{0.375}Fe_2O_4$ after photocatalytic treatment.

Table 4 Summary of the pseudo-first-order kinetics for the photo-catalytic MB dye degradation using different $Zn_{1-x}Co_{0.5x}Mg_{0.5x}Fe_2O_4$ ferrites

Catalyst	k (min^{-1})	R^2
ZF	0.032	0.94
ZCMF1	0.039	0.94
ZCMF2	0.054	0.95
ZCMF3	0.108	0.99
CMF	0.072	0.98

in stability and reusability. In addition, as seen in Fig. 8d, the $Zn_{0.25}Co_{0.375}Mg_{0.375}Fe_2O_4$ XRD was performed before and after the photocatalytic degradation reaction of the MB dye. It is worth noting that after four consecutive cycles, the $Zn_{0.25}Co_{0.375}Mg_{0.375}Fe_2O_4$ XRD pattern has almost no difference, which further shows that it has outstanding reliability and reusability.

Based on the above results (Fig. 9a), we proposed the pho-tocatalytic mechanism using $Zn_{0.25}Co_{0.375}Mg_{0.375}Fe_2O_4$ under sunlight irradiation. Initially, the sunlight falls on the $Zn_{0.25}Co_{0.375}Mg_{0.375}Fe_2O_4$ photocatalyst surface, activating the ferrite, and pairs of e^-/h^+ are formed. The electrons in the $Zn_{0.25}Co_{0.375}Mg_{0.375}Fe_2O_4$ valence band become excited as the holes are left in the valence band. The holes are used for the oxidation process in the valence band, while the electrons are used for the reduction process in the conduction band. The reactive species ($OH^•$, $O_2^{-•}$) that are produced decay the meth-ylene blue dye in CO_2 and H_2O.[46] In this degradation, the hydroxyl ion plays a significant role in the photodegradation of the methylene blue dye. The presence and absence of the hydroxyl radical scavenger, such as isopropyl alcohol, was monitored to investigate the development of a photo-degradation reaction. The rate constant decreased significantly with the inclusion of 0.1 mL of IPA, as shown in Fig. 9b. The photodegradation of the MB dye in the presence of $Zn_{0.25}Co_{0.375}Mg_{0.375}Fe_2O_4$ and sunlight is responsible for promoting the formation.

The bandgap of the ferrites $Zn_{1-x}Co_{0.5x}Mg_{0.5x}Fe_2O_4$ lies in the visible light field (2.01–2.43 eV), which is known from optical measurements. As described in the optical properties section, the narrowing of the bandgap of ZnCMF3 was respon-sible for the greater activity. This makes the band structure of ZnCMF3 better for solar light optical absorption, as well as charge carrier separation. As a result, ZnCMF3 exhibits stronger MB dye degradation over other ferrites. In addition, the VSM study of the ZnCMF3 ferrites reveals that the increased cobalt
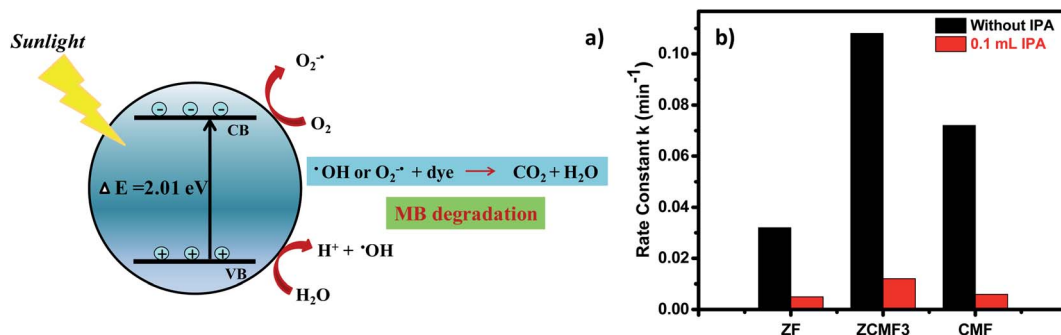
Fig. 9 (a) Possible mechanism for the photocatalytic MB dye degradation under sunlight irradiation using $Zn_{0.25}Co_{0.375}Mg_{0.375}Fe_2O_4$. (b) Effect of the IPA scavenger on the photodegradation efficiency of methylene blue using $Zn_{0.25}Co_{0.375}Mg_{0.375}Fe_2O_4$.

Table 5 Comparison of previous research reports of methylene blue dye degradation using ferrites

Sr. no.	Photocatalysts material used	Dye soln. tested	Optimized catalyst & quantity	Light source used	Remark	References
1	$MnFe_2O_4/rGO$	10 ppm MB dye	0.03 g	40 W UV lamp	97% degradation within 60 min	Mandal et al.;[42]
2	$CoFe_2O_4$	10 ppm MB dye	0.01 g	Visible light	80% degradation in 140 min	Kalam et al.;[43]
3	$ZnO/ZnFe_2O_4$	10 ppm MB dye	0.08 g	300 W Xe arc lamp (UV & visible light)	98% degradation in 240 min	Yan Xu et al.;[47]
4	$ZnFe_2O_4/Fe_2O_3$	10 ppm MB dye	0.5 g	75 W Hg lamp as UV source	88.27% degradation in 120 min	Cao et al.;[22]
5	$Zn_{1-x}Co_{0.5x}Mg_{0.5x}Fe_2O_4$	10 ppm MB dye	0.2 g	Sunlight	99% degradation 40 min	Current work

ions in the octahedral sites are responsible for the high photocatalytic activity. More precisely, the MB degradation of ZnCMF3 is much higher than in previous studies (Table 5).[22,42,43,47]

4. Conclusion

The present study reports the synthesis of $Zn_{1-x}Co_{0.5x}Mg_{0.5x}$-$Fe_2O_4$ ferrites through the sol–gel auto combustion method. The $Zn_{1-x}Co_{0.5x}Mg_{0.5x}Fe_2O_4$ ferrites demonstrate high photocatalytic activity under sunlight irradiation for the degradation of the MB dye. Different characterization techniques characterized the prepared $Zn_{1-x}Co_{0.5x}Mg_{0.5x}Fe_2O_4$ ferrites, which confirmed the formation of the single-phase cubic spinel structure with space group $Fd3m$. When compared to other ferrites, the $Zn_{0.25}Co_{0.375}Mg_{0.375}Fe_2O_4$ ferrite displays excellent degradation capability for the MB dye. The $Zn_{0.25}Co_{0.375}$-$Mg_{0.375}Fe_2O_4$ ferrite could be regenerated up to four times with the photocatalytic output negligibly degrading. The present low-cost magnetic recyclable $Zn_{0.25}Co_{0.375}Mg_{0.375}Fe_2O_4$ ferrite can be used to mitigate the multi-industry environmental problems.

Conflicts of interest

There are no conflicts to declare.

Acknowledgements

References

1 S. Agrawal, A. Parveen and A. Azam, Structural, electrical, and optomagnetic tweaking of Zn doped $CoFe_{2-x}Zn_xO_{4-\delta}$ nanoparticles, J. Magn. Magn. Mater., 2016, 414, 114–152.

2 C. Singh, S. Jauhar, V. Kumar, J. Singh and S. Singhal, Synthesis of zinc substituted cobalt ferrites via reverse micelle technique involving in situ template formation: a study on their structural, magnetic, optical and catalytic properties, Mater. Chem. Phys., 2015, 156, 188–197.

3 U. Salazar-Kuri, J. O. Estevez, N. R. Silva-González, Y. Pal and M. E. Mendoza, Structure and magnetic properties of the $Co_{1-x}Ni_xFe_2O_4$-$BaTiO_3$ core-shell nanoparticles, J. Magn. Magn. Mater., 2017, 442, 247–254.

4 C. Singh, A. Goyal and S. Singhal, Nickel-doped cobalt ferrite nanoparticles: efficient catalysts for the reduction of nitroaromatic compounds and photo-oxidative degradation of toxic dyes, Nanoscale, 2014, 6, 7959–7970.

5 P. Xiong, C. Hu, Y. Fan, W. Zhang, J. Zhu and X. Wang, Ternary manganese ferrite/graphene/polyaniline nanostructure with enhanced electrochemical capacitance performance, J. Power Sources, 2014, 266, 384–392.

6 H. Yang, C. Zhang, X. Shi, H. Hu, X. Du, Y. Fang, Y. Ma, H. Wu and S. Yang, Water soluble superparamagnetic

manganese ferrite nanoparticles for magnetic resonance imaging, *Biomaterials*, 2010, **31**, 3667–3673.

7 A. Samavati and A. F. Ismail, Antibacterial properties of copper-substituted cobalt ferrite nanoparticles synthesized by co-precipitation method, *Particuology*, 2017, **30**, 158–163.

8 W. Chen, D. Liu, W. Wu, H. Zhanga and J. Wua, Structure and magnetic properties evolution of rod-like $Co_{0.5}Ni_{0.25}Zn_{0.25}Dy_xFe_{2-x}O_4$ synthesized by solvothermal method, *J. Magn. Magn. Mater.*, 2017, **422**, 49–56.

9 R. Sharma, P. Thakur, M. Kuma, N. Thakur, N. S. Negi, P. Sharma and V. Sharma, Improvement in magnetic behaviour of cobalt doped magnesium zinc nano-ferrites via coprecipitation route, *J. Alloys Compd.*, 2016, **684**, 569–581.

10 G. Theopil Anand, L. J. Kennedy, J. J. Vijaya, K. Kaviyarasan and M. Sukumar, Structural, optical and magnetic characterization of $Zn_{1-x}Ni_xAl_2O_4$ ($0 \leq x \leq 0.5$) spinel nanostructures synthesized by microwave combustion technique, *Ceram. Int.*, 2015, **41**, 603–615.

11 M. Atif and M. Nadeem, Sol-gel synthesis of nanocrystalline $Zn_{1-x}Ni_xFe_2O_4$ ceramics and its structural, magnetic and dielectric properties, *J. Sol-Gel Sci. Technol.*, 2014, **72**, 615–626.

12 M. Ikram, M. I. Khan, A. Raza, M. Imran, A. Ul-Hamid and S. Ali, Outstanding performance of silver-decorated MoS_2 nano petals used as nano catalyst for synthetic dye, *Phys. E*, 2020, **124**, 114246.

13 A. Raza, U. Qumar, J. Hassan, M. Ikram, A. Ul-Hamid, J. Haider, M. Imran and S. Ali, A comparative study of dirac 2D materials, TMDCs and 2D insulators with regard to their structures and photocatalytic/sonophotocatalytic behavior, *Appl. Nanosci.*, 2020, **10**, 3875–3899.

14 M. Manzoor, A. Rafiq, M. Ikram, *et al.*, Structural, optical, and magnetic study of Ni-doped TiO_2 nanoparticles synthesized by sol–gel method, *Int. Nano Lett.*, 2018, **8**, 1–8.

15 M. Khademalrasool, M. D. Talebzadeh and M. Farbod, ZnO/Silver Nanocubes Nanocomposites: Preparation, Characterization, and Scrutiny of Plasmon-Induced Photocatalysis Activity, *J. Photochem. Photobiol., A*, 2020, **396**, 112561.

16 S. Balgude, S. Barkade and S. Mardikar, Metal Oxides for High-Performance Hydrogen Generation by Water Splitting, *Multifunctional Nanostructured Metal Oxides for Energy Harvesting and Storage Devices*, 2020, DOI: 10.1201/9780429296871-6.

17 B. Sahoo, S. Kumar Sahu, S. Nayak, D. Dhara and P. Pramanik, Fabrication of magnetic mesoporous manganese ferrite nanocomposites as efficient catalyst for degradation of dye pollutants, *Catal. Sci. Technol.*, 2012, **2**, 1367–1374.

18 S. Chandrasekaran, C. Bowen, P. Zhang, Z. Li, Q. Yuan, X. Ren and L. Deng, Spinel photocatalysts for environmental remediation, hydrogen generation, CO_2 reduction and photoelectrochemical water splitting, *J. Mater. Chem. A*, 2018, **6**, 11078–11104.

19 S. Kapoor, A. Goyal, S. Bansal and S. Singhal, Emergence of bismuth substituted cobalt ferrite nanostructures as versatile candidates for the enhanced oxidative degradation of hazardous organic dyes, *New J. Chem.*, 2018, **42**, 14965–14977.

20 F. Chang, Z. Chen, J. Jing and J. Hou, The photocatalytic phenol degradation mechanism of Ag-modified ZnO nanorods, *J. Mater. Chem. C*, 2020, **8**, 3000–3009.

21 S. Balgude, Y. Sethi, A. Gaikwad, B. Kale, D. Amalnerkar and P. Adhyapak, Unique N doped Sn_3O_4 nanosheets as an efficient and stable photocatalyst for hydrogen generation under sunlight, *Nanoscale*, 2020, **12**, 8502–8510.

22 Z. Cao, J. Zhang, J. Zhou, X. Ruan, D. Chen, J. Liu, Q. Liu and G. Qian, Electroplating sludge derived zinc-ferrite catalyst for the efficient photo-Fenton degradation of dye, *J. Environ. Manage.*, 2017, **193**, 146–153.

23 Li Yang, D. Chen, S. Fan and T. Yang, Enhanced visible light assisted Fenton-like degradation of dye via metal-doped zinc ferrite nanosphere prepared from metal-rich industrial wastewater, *J. Taiwan Inst. Chem. Eng.*, 2019, **96**, 185–192.

24 M. H. Habibi and J. Parhizkar, Cobalt ferrite nano-composite coated on glass by Doctor Blade method for photo-catalytic degradation of an azo textile dye Reactive Red 4: XRD, FESEM and DRS investigations, *Spectrochim. Acta, Part A*, 2015, **150**, 879–885.

25 A. I. Borhan, P. Samoila, V. Hulea, A. R. Iordan and M. N. Palamaru, Effect of Al^{3+} substituted zinc ferrite on photocatalytic degradation of Orange I azo dye, *J. Photochem. Photobiol., A*, 2014, **279**, 17–23.

26 N. M. Mahmoodi, Zinc ferrite nanoparticle as a magnetic catalyst: synthesis and dye degradation, *Mater. Res. Bull.*, 2013, **48**, 4255–4260.

27 S. C. W. Sakti, R. N. Laily, S. Aliyah, N. Indrasari, M. Z. Fahmi, H. V. Lee, Y. Akemotod and S. Tanaka, Re-collectable and recyclable epichlorohydrin-cross linked humic acid with spinel cobalt ferrite core for simple magnetic removal of cationic triarylmethane dyes in polluted water, *J. Environ. Chem. Eng.*, 2020, **8**, 104004.

28 A. Wahab, M. Imran, M. Ikram, *et al.*, Dye degradation property of cobalt and manganese doped iron oxide nanoparticles, *Appl. Nanosci.*, 2019, **9**, 1823–1832.

29 H. O'neill and S. C. Hugh, Temperature dependence of the cation distribution in zinc ferrite ($ZnFe_2O_4$) from powder XRD structural refinements, *Eur. J. Mineral.*, 1992, **4**, 571–580.

30 H. P. Klung and L. E. Alexander, Synthesis of Ni-Zn ferrite catalysts by combustion reaction using different fuels, *X-ray diffraction procedures for polycrystalline and amorphous materials*, Wiley, New York, NY 1997, p. 637.

31 T. R. Tatarchuk, M. Bououdina, N. D. Paliychuk, I. P. Yaremiy and V. V. Moklyak, Structural characterization and antistructure modeling of cobalt substituted zinc ferrites, *J. Alloys Compd.*, 2017, **694**, 777–791.

32 R. Sharma, P. Thakur, P. Sharma and V. Sharma, Ferrimagnetic Ni^{2+} doped Mg-Zn spinel ferrite nanoparticles for high density information storage, *J. Alloys Compd.*, 2017, **704**, 7–17.

33 A. K. M. Akther Hossaina, K. Khirul Kabira, M. Sekib, T. Kawaib and H. Tabatab, Structural, AC, and DC magnetic properties of $Zn_{1-x}Co_xFe_2O_4$, *J. Phys. Chem. Solids*, 2007, **68**, 1933–1939.

34 L. Weil, F. Bertaut and L. Bochirol, Magnetic properties and structure of the quadratic phase of copper ferrite, *J. Phys. Radium*, 1950, **11**, 208–212.

35 R. Sharma and S. Singhal, Structural, magnetic and electrical properties of zinc doped nickel ferrite and their application in photo catalytic degradation of methylene blue, *Phys. B*, 2013, **414**, 83–90.

36 M. A. Amer, A. Tawfiq, A. G. Mostafa, A. F. El-Shora and S. M. Zaki, Spectral studies of Co substituted Ni–Zn ferrites, *J. Magn. Magn. Mater.*, 2011, **323**, 1445–1452.

37 R. D. Waldron, Infrared Spectra of Ferrites, *Phys. Rev.*, 1955, **99**, 1727–1735.

38 V. Rathod, A. V. Anupama, R. Vijaya Kumar, V. M. Jali and B. Sahoo, correlated vibrations of the tetrahedral and octahedral complexes and splitting of the absorption bands in FTIR spectra of Li-Zn ferrites, *Vib. Spectrosc.*, 2017, **92**, 267–272.

39 Y. Tang, X. Wang, Q. Zhang, Y. Li and H. Wang, Solvothermal synthesis of $Co_{1-x}Ni_xFe_2O_4$ nanoparticles and its application in ammonia vapors detection, *Prog. Nat. Sci.: Mater. Int.*, 2012, **22**, 53–58.

40 T. R. Tatarchuk, N. D. Paliychuk, M. Bououdina, B. Al-Najar, M. Pacia, W. Macyk and A. Shyichuk, Effect of cobalt substitution on structural, elastic, magnetic and optical properties of zinc ferrite nanoparticles, *J. Alloys Compd.*, 2018, **731**, 1256–1266.

41 K. Jangam, K. Patil, S. Balgude, S. Patange and P. More, Synthesis and characterization of magnetically separable $Zn_{1-x}Co_xFeMnO_4$ nanoferrites as highly efficient photocatalyst for degradation of dye under solar light irradiation, *J. Phys. Chem. Solids*, 2020, 109700.

42 B. Mandal, J. Panda, P. K. Paul, R. Sarkar and B. Tudu, $MnFe_2O_4$ decorated reduced graphene oxide heterostructures: nanophotocatalyst for methylene blue dye degradation, *Vaccum*, 2020, **173**, 109150–109158.

43 A. Kalam, A. G. Al-Sehemi, M. Assiri, G. Du, T. Ahmad, I. Ahmad and M. Pannipara, Modified Solvothermal synthesis of cobalt ferrite ($CoFe_2O_4$) magnetic nanoparticles photocatalysts for degradation of methylene blue with H_2O_2/visible light, *Results Phys.*, 2018, **8**, 1046–1053.

44 F. Almeida, E. C. Grzebielucka, S. R. M. Antunes, C. P. F. Borges, A. V. C. Andrade and E. C. F. Souza, Visible light activated magnetic photocatalysts for water treatment, *J. Environ. Manage.*, 2020, **273**, 111143–111152.

45 K. N. Harish, H. S. B. Naik, P. N. P. Kumar and R. Viswanath, Optical and Photocatalytic Properties of Solar Light Active Nd-Substituted Ni Ferrite Catalysts: For Environmental Protection, *ACS Sustainable Chem. Eng.*, 2013, **1**(9), 1143–1153.

46 S. Balgude, Y. Sethi, B. Kale, D. Amalnerkar and P. Adhyapak, ZnO decorated Sn_3O_4 nanosheets nano-heterostructure: stable photocatalyst for water splitting and dye degradation under natural sunlight, *RSC Adv.*, 2019, **9**, 10289–10296.

47 Y. Xu, S. Wu, X. Li, Y. Huang, Z. Wang, Y. Han, J. Wu, H. Meng and X. Zhang, Synthesis, characterization and their photocatalytic degradation properties of $ZnO/ZnFe_2O_4$ magnetic heterostructures, *New J. Chem.*, 2017, **41**, 15433–15438.